

# Spontaneous Reshaping and Splitting of AgCl Nanocrystals under Electron Beam Illumination

Xuezheng Tian, Utkarsh Anand, Utkur Mirsaidov, and Haimei Zheng\*

AgCl is photosensitive and thus often used as micromotors. However, the dynamics of individual AgCl nanoparticle motion in liquids upon illumination remains elusive. Here, using liquid cell transmission electron microscope (TEM), AgCl nanocrystals reshaping and splitting spontaneously in an aqueous solution under electron beam illumination are observed. It is found that the AgCl nanocrystals are negatively charged in the liquid environment, where the charge induces a repulsive Coulomb force that reshapes and stretches those nanocrystals. Upon extensive stretching, the AgCl nanocrystal splits into small nanocrystals and each nanocrystal retracts back into cuboid shapes due to the cohesive surface. This analysis shows that each nanocrystal maintains a single crystal rocksalt structure during splitting. The splitting of AgCl nanocrystals is analogous to the electrified liquid droplets or other reported the Coulomb fission phenomenon, but with distinctive structural properties. Revealing of the dynamic behavior of AgCl nanocrystals opens the opportunity to explore their potential applications as actuators for nanodevices.

## 1. Introduction

AgCl is photosensitive, thus micrometer-sized AgCl particles have frequently been reported as photoactivated micromotors, which convert photon energy into mechanical energy to produce motion.<sup>[1–4]</sup> For instance, upon ultra-violet (UV) light illumination, AgCl particles immersed in water decompose into Ag and hydrochloric acid (HCl). The produced protons diffuse much faster than chloride ions ( $D_{H^+} = 9.311 \times 10^{-5} \text{ cm}^2 \text{ s}^{-1}$ ,  $D_{Cl^-} = 1.385 \times 10^{-5} \text{ cm}^2 \text{ s}^{-1}$ ), resulting in an electrolyte gradient, which generates an electric field.<sup>[5,6]</sup> The electrolyte gradient leads to ionic diffusiophoresis, which provides a driving force for the nanoparticles to move. Asymmetric photodecomposition may cause directional particle motion.<sup>[7,8]</sup> The reduced Ag metal can be plated onto the particles as the AgCl are consumed in the above experiments, which slows

down the nanoparticle motion. It has also been reported that when  $H_2O_2$  is added to the AgCl–UV light system, the reduction of AgCl to Ag by UV light and the oxidation of Ag to AgCl by peroxide produce and consume HCl. This competition and the associated gradient reversal lead to periodic attraction and repulsion between colloids, thus oscillatory motion of the particles.<sup>[9]</sup> The facile chemical conversion of AgCl particles and the associated dynamic motion are fascinating. However, little is known about structural instability and motion of AgCl nanoparticles in liquids due to the lack of direct observation with high spatial resolution.

Here, we report the spontaneous reshaping and splitting of AgCl nanocrystals in an aqueous solution induced by electron beam illumination, which are achieved using in situ liquid cell transmission electron microscopy (TEM). A nanofabricated liquid cell from silicon wafers is composed of two liquid reservoirs and an electron transparent  $SiN_x$  membrane window (each membrane is 20 nm thick). We load the precursor solution of  $10\text{--}100 \times 10^{-3} \text{ M}$  KCl aqueous solution with Ag nanoparticles into one of the reservoirs and the solution is drawn into the cell by capillary force forming a thin liquid layer sandwiched between the  $SiN_x$  membranes<sup>[10–13]</sup> (see Experimental Section). AgCl nanocrystals are formed under electron beam irradiation. All AgCl nanocrystals are more or less faceted nanocuboids with rectangles or deformed rectangles in the two-dimensional projection (see Sections S1 and S2, Supporting

Dr. X. Tian, Prof. H. Zheng  
Materials Sciences Division  
Lawrence Berkeley National Laboratory  
Berkeley, CA 94720, USA  
E-mail: hmzheng@lbl.gov


Dr. X. Tian, Prof. H. Zheng  
Department of Materials Science and Engineering  
University of California  
Berkeley, CA 94720, USA

Dr. X. Tian, Prof. H. Zheng  
Berkeley Education Alliance for Research in Singapore  
Singapore 138602, Singapore

U. Anand, Prof. U. Mirsaidov  
Centre for BioImaging Sciences  
Department of Biological Sciences  
National University of Singapore  
Singapore 117557, Singapore

U. Anand, Prof. U. Mirsaidov  
Department of Physics  
National University of Singapore  
Singapore 117551, Singapore

U. Anand, Prof. U. Mirsaidov  
Centre for Advanced 2D Materials and Graphene Research Centre  
National University of Singapore  
Singapore 117546, Singapore

 The ORCID identification number(s) for the author(s) of this article can be found under <https://doi.org/10.1002/smll.201803231>.

DOI: 10.1002/smll.201803231

Information). AgCl nanocrystals become unstable under electron beam illumination. When the electron dose rate is above a certain threshold, they undergo drastic reshaping and splitting events. More than a hundred splitting events are observed, of which we record movies at the rate of 10 frames per second. The electron beam dose rate is maintained at  $0\text{--}40\text{ e}^-(\text{\AA}^2\text{ s})^{-1}$  as specified in each case.

## 2. Spontaneous Reshaping and Splitting of AgCl Nanocrystals

The schematic in **Figure 1a** shows a typical splitting event of a AgCl nanocrystal revealed through liquid cell TEM. There are three stages during the splitting event: lateral stretching

of the AgCl nanocrystal preferred at the corner(s), splitting of the primary nanocrystal, and retracting of the secondary AgCl nanocrystals into nanocuboids. **Figure 1b,c** show two typical splitting events stretching out from the corners of AgCl nanocrystals, which are abrupt and explosive. More examples of explosive splitting are available in Section S5 (Supporting Information). It is noted that all of those explosive splitting events are initiated at the nanocrystal corners. The projected size of the AgCl nanocrystal increases up to three times of the original size during the stretching, as shown by the size evolution plotted in **Figure 1e,f**. Subsequently, splitting of the AgCl nanocrystal is observed. After splitting, all secondary nanocrystals retract into rectangular shapes. From the observation, we hypothesize that two counterbalanced forces are regulating the reshaping and splitting process, i.e., a repulsive force that

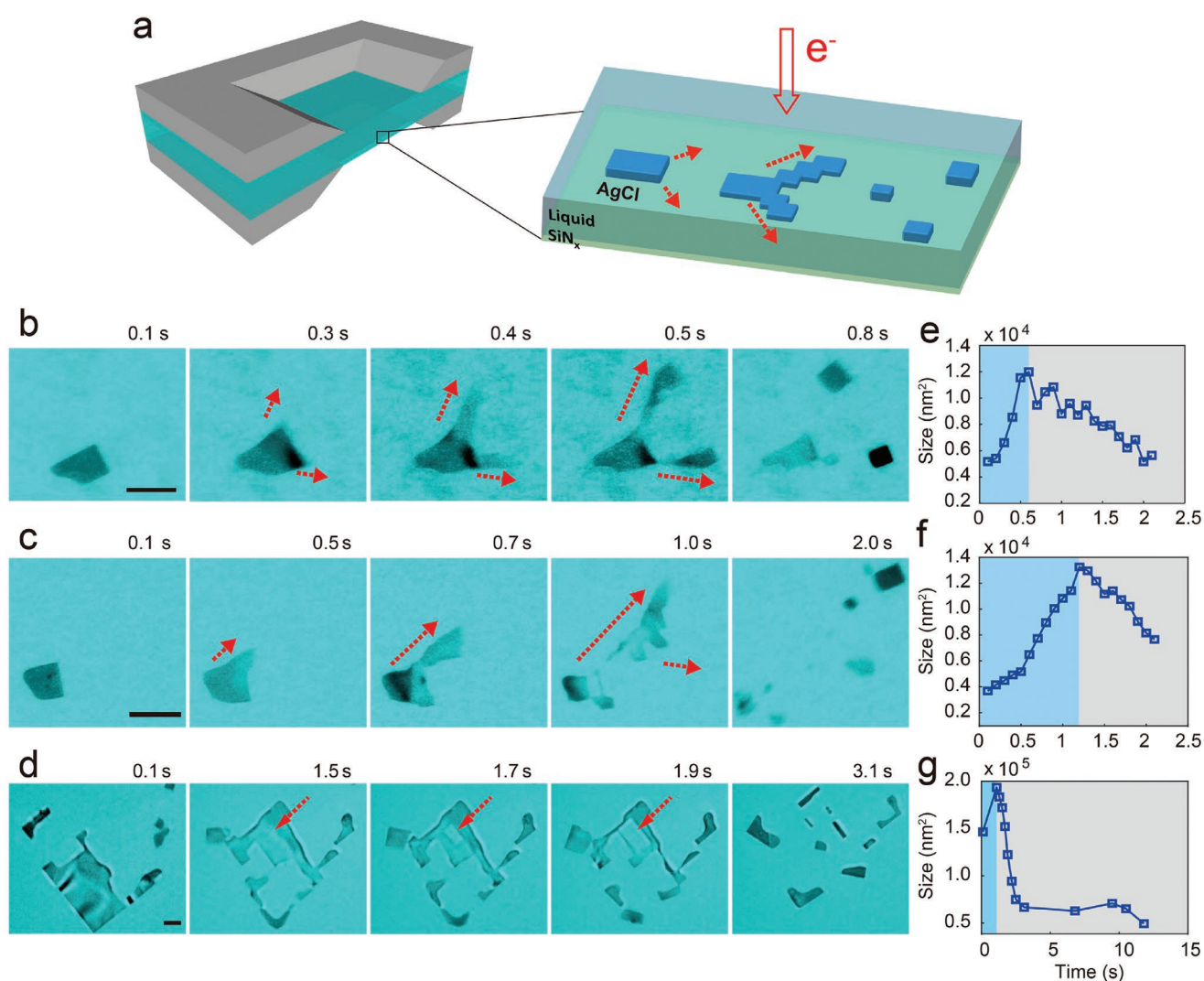


**Figure 1.** Typical spontaneous reshaping and splitting of AgCl nanocrystals in liquid cell under electron beam illumination. a) Schematic representation of stretching, splitting, and retraction of AgCl nanocrystal during a splitting event. b) Sequential TEM images showing the explosive splitting starting from two corners of a AgCl nanocrystal. The red arrows show the nanocrystal stretching directions during the splitting process. c) Sequential TEM images showing the explosive splitting from one corner of a AgCl nanocrystal. d) A gradual splitting event initiated from the interior of a AgCl nanocrystal. The red arrow indicates the initial splitting points. e–g) The projected size evolution with time for the corresponding nanocrystals shown in (b–d). All scale bars are 100 nm. Electron dose rate was maintained at  $13\text{ e}^-(\text{\AA}^2\text{ s})^{-1}$  for the above cases.

stretches the nanocrystals and a cohesive force that retracts the AgCl nanocrystals. We will discuss the origin of this driving force further in detail in a later section of this paper.

Another type of splitting without the explosive characteristics is also observed, which is associated with much larger AgCl nanocrystals. Figure 1d shows a large AgCl nanocrystal (length/height  $\approx 385$  nm) expands from the interior by first forming holes, then holes become larger, and the nanocrystal eventually splits into many pieces. The holes are accounted to the weak points induced by radiolysis. After splitting, each piece transforms from the irregular shape into a nanocuboid and is stabilized. Comparing with the typical explosive processes, those mild splitting events exhibit three stages: premature stretching, splitting from edge or interior weak region, and retraction. The overall effect is the same with explosive splitting: to re-allocate the charges (decreasing the Coulomb energy), and increase the total surface area (increasing surface energy). Finally the system is stabilized, but through a different splitting approach.

### 3. AgCl Nanocrystals Are Single Crystalline and Change Shape Like Liquids

The facile processes of AgCl nanocrystal reshaping, splitting, and retracting highlight the fluidity of AgCl nanocrystals. Considering that AgCl nanocrystal reshaping and merging are an intraparticle atomic diffusion process, we can estimate the viscosity of the AgCl nanocrystals with a simplified model using Stokes equation. Taking the merging of two nanocrystals in Figure 2a as an example, the merging process is regarded as a self-diffusion process with a finite velocity ( $\approx 50$  nm s<sup>-1</sup>), where Stokes dragging force is counter balanced by surface tension. With measured nanocrystal size, merging velocity and estimated surface tension ( $0.35$  J m<sup>-2</sup>),<sup>[14]</sup> the viscosity of

the merging nanocrystal is estimated to be  $2.3 \times 10^6$  Pa s (see Section S6, Supporting Information for details). Similarly, Figure 2b shows a large nanocrystal splits, and the secondary pieces retract with a finite retraction velocity, which can be used to estimate the dynamic viscosity. The viscosity of  $3.9 \times 10^5$  Pa s is achieved in this case. Therefore, the viscosity of AgCl in this experiment is in the order of  $10^5$ – $10^6$  Pa s, which is within the range of molten glass.<sup>[15]</sup> AgCl is known to be radiation sensitive and has been used in photographic films. Under electron beam irradiation, ionic bonding between Ag<sup>+</sup> and Cl<sup>-</sup> ions are broken due to radiolysis resulting in silver reduction.<sup>[16]</sup> The observed liquid-like behaviors of the AgCl nanocrystals arises from the massive bond breaking due to electron beam induced radiolysis.

We have taken selected area electron diffraction (SAED) patterns during the nanocrystal reshaping and splitting processes. Figure 3 shows a nanocrystal (P) splits into three (P, Q, and R) pieces and the corresponding electron diffraction patterns at different stages. The original AgCl nanocrystal (P) is single crystalline along [001] zone axis (time 32.0 s). After splitting, three independent diffraction patterns corresponding to each individual AgCl nanocrystals (P, Q, and R) are achieved (time 35.5 s). Each nanocrystal is single crystalline with face-centered cubic (FCC) rocksalt structure and the primary (100) terminating facets. This has been confirmed by additional measurements of a large number of nanocrystals (see Figure S2 in Supporting Information), which is consistent with the crystal habit of AgCl nanocrystals.<sup>[16]</sup> The orientation of diffraction patterns matches the shape of each AgCl nanocrystal very well, as shown in Figure 3b,c. When the nanocrystal P rotates 10° clockwise (from time 35.5 s to 39.8 s), the corresponding diffraction of P also rotates by the same angle; the nanocrystal Q and R remain stationary, their diffraction patterns also remain stationary.

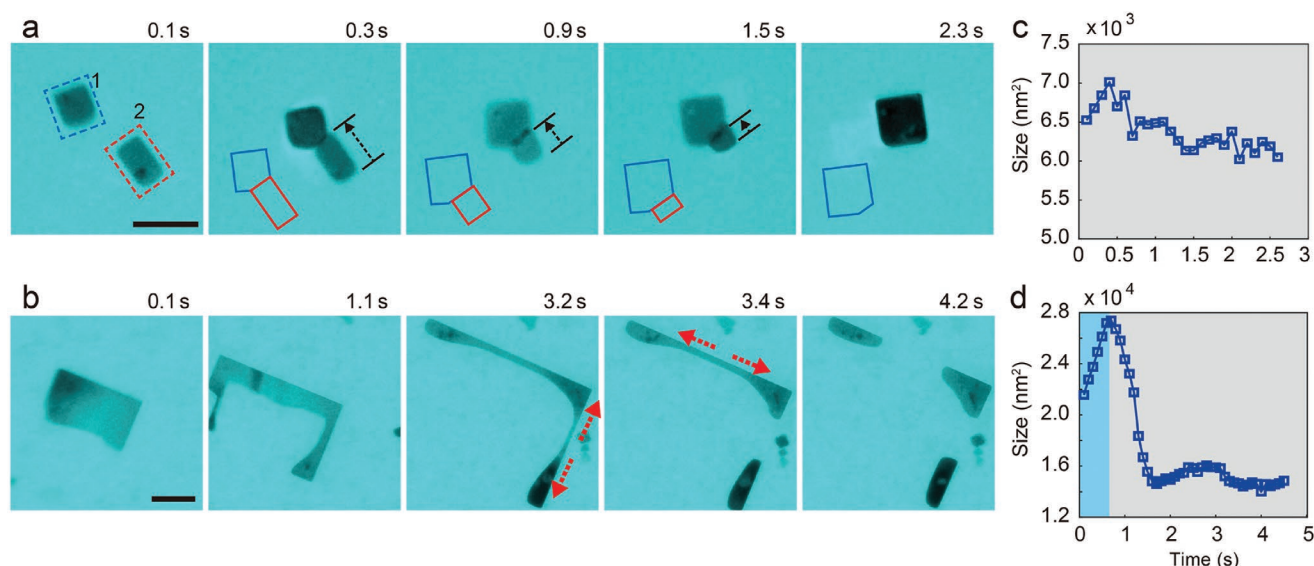


**Figure 2.** Merging and stretching of AgCl nanocrystals show the liquid-like behavior of nanocrystals. a) Two AgCl nanocrystals merging together with a finite merging velocity of  $50$  nm s<sup>-1</sup>. Using Stokes equation, the dynamic viscosity here is estimated to be  $2.3 \times 10^6$  Pa s. b) A large nanocrystal stretching and splitting into pieces with a finite splitting velocity. The maximum retracting speed is about  $300$  nm s<sup>-1</sup>. The dynamic viscosity here is estimated to be  $3.9 \times 10^5$  Pa s. c,d) Size evolution corresponding to the dynamic processes in (a) and (b), respectively. The scale bars are  $100$  nm.



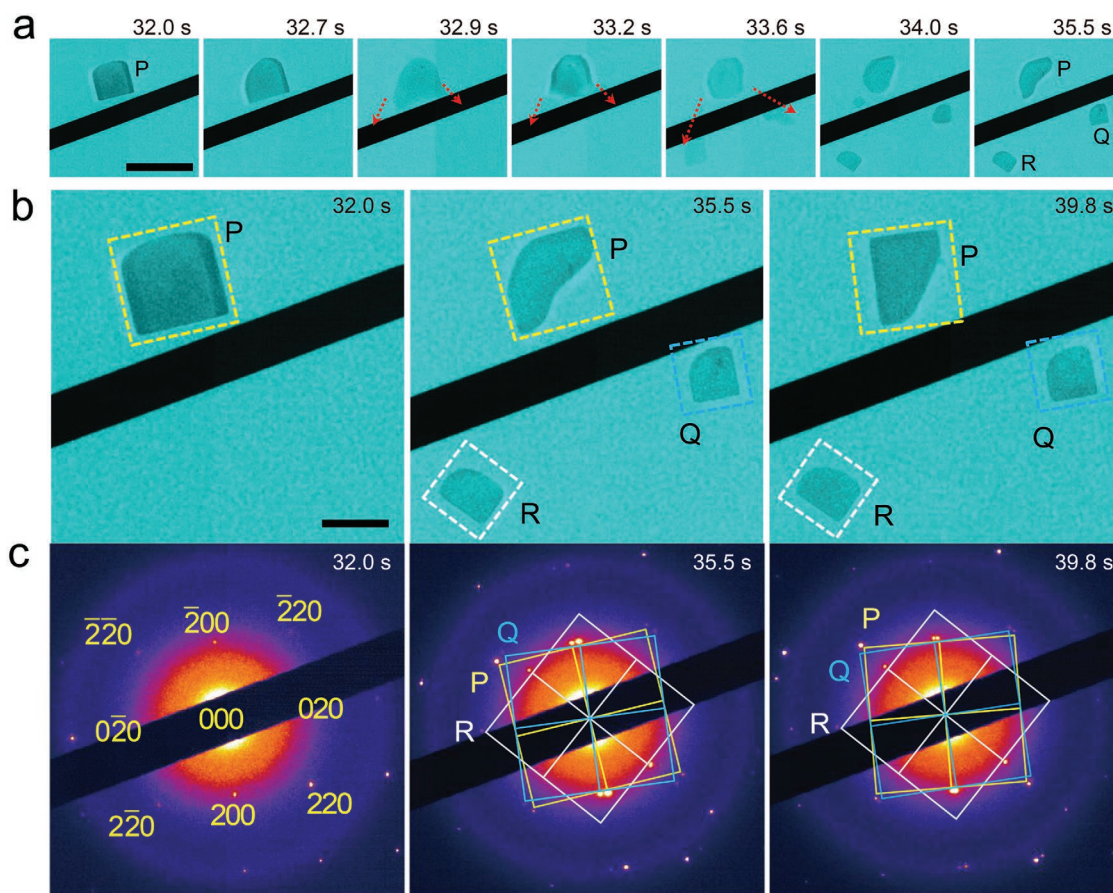


**Figure 3.** AgCl nanocrystals maintain single crystalline structure during splitting. a) Sequential TEM images showing a typical splitting event initiated from two corners of the nanocrystal. Arrows indicate splitting directions. The black bar in the middle is the beam stopper. During the splitting process, the electron dose rate is manipulated between 4 and 13  $\text{e} (\text{\AA}^2 \text{s})^{-1}$ . Scale bar is 500 nm. b) TEM images showing different states of splitting event, where the nanocrystal “P” splits into “P,” “Q,” and “R.” Edges of the surrounding boxes are parallel to the nanocrystal straight edges. The colors of the boxes are consistent with the electron diffraction patterns in (c). Scale bar is 200 nm. c) Each electron diffraction pattern corresponding to the contributing nanocrystals in (b): P, Q, and R. The Bragg spots are all indexed to be AgCl with the lattice constant of 5.55 Å and along [001] zone axis.

#### 4. Rayleigh Instability and Coulomb Fission

We further find that AgCl nanocrystals reshaping is highly dependent on the electron dose rate. In Figure 4a, the morphology of five nanocrystals with various sizes can be manipulated between near the spherical nanoparticles and the faceted cuboids by changing the electron dose rate. Under low electron dose rate ( $1 \text{ e} (\text{\AA}^2 \text{s})^{-1}$ ), surface tension dominates thus the nanocrystals with rounded corners are observed. Higher electron dose rate ( $5 \text{ e} (\text{\AA}^2 \text{s})^{-1}$  or higher) induces nanocrystals with more well-defined corners. Figure 4b shows the shape evolution of a AgCl nanocrystal highlighting the electron dose effects. Under high electron dose rate ( $13 \text{ e} (\text{\AA}^2 \text{s})^{-1}$ ), the nanocrystal is highly stretched with an irregular shape (time 0.1–5.9 s). When the electron dose rate decreases to  $1 \text{ e} (\text{\AA}^2 \text{s})^{-1}$ , the nanocrystal quickly retracts into a single rounded nanoparticle (time 6.0–6.4 s). This suggests that the repulsive force counter-balancing the surface tension decreases with a lower electron dose rate.

Figure 4c shows statistics of the nanocrystal sizes in various splitting events under different electron dose rates. Large nanocrystals (e.g., edge length over 200 nm) may split under

significantly lower electron dose rate ( $\approx 3 \text{ e} (\text{\AA}^2 \text{s})^{-1}$ ). Smaller nanocrystals require a higher dose rate to split. Various of splitting events are observed under the electron dose rate of 0–35  $\text{e} (\text{\AA}^2 \text{s})^{-1}$ . Nanocrystals smaller than 30 nm do not split under even much higher electron dose rate ( $>40 \text{ e} (\text{\AA}^2 \text{s})^{-1}$ ). It is also noted that electron-beam-induced reduction of AgCl into Ag clusters is found when the electron dose rate is above  $40 \text{ e} (\text{\AA}^2 \text{s})^{-1}$  (see Section S10, Supporting Information). However, when the electron dose rate is below  $40 \text{ e} (\text{\AA}^2 \text{s})^{-1}$ , no obvious decomposition of AgCl nanocrystals is observed. It is also noted that many AgCl nanoparticles move in the same direction within the field of view, which is likely due to the fluid flow or an electric field gradient from inhomogeneous electron beam density.

Electron beam is known to influence a sample in multiple ways, including heating, charging, exerting radiation pressure and photochemical reactions (see Sections S8–S10, Supporting Information).<sup>[17,18]</sup> We consider the electron beam induced radiolysis and the accompanied charging effects are responsible for the observed reshaping and splitting of the AgCl nanocrystals. The AgCl nanocrystal surface in KCl solution can be highly

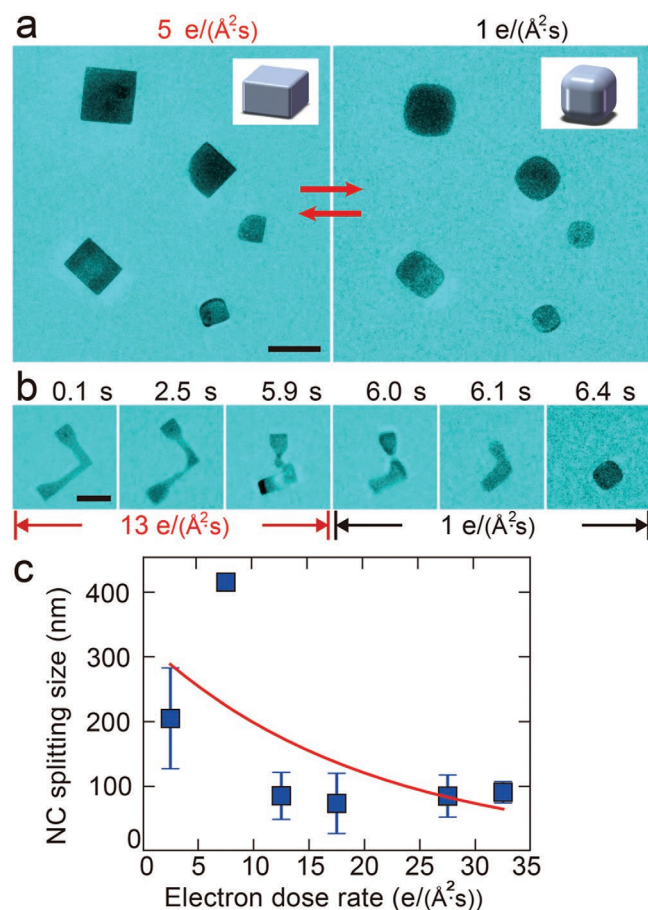
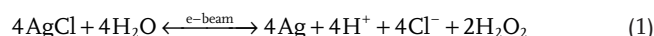


**Figure 4.** The electron dose rate dependent AgCl reshaping and splitting. a) Reversible morphological changes dependent on the electron beam dose rate. b) AgCl nanocrystal stretches and splits under high electron beam dose rate ( $13 \text{ e } (\text{\AA}^2 \text{ s}^{-1})$ ) and retracts into a round nanoparticle under low electron beam dose rate ( $1 \text{ e } (\text{\AA}^2 \text{ s}^{-1})$ ). All scale bars are 100 nm. c) Statistics of nanocrystal (NC) sizes in various splitting events under different electron dose rates.

negatively charged due to  $\text{Cl}^-$  adsorption, which is modulated by radiolysis related redox reactions.<sup>[16]</sup> Thus, a repulsive electrostatic force can be generated which stretches the AgCl nanocrystal. Simultaneously, the surface tension retracts the nanocrystal. The interplay between these two factors induces the rich dynamics of AgCl nanocrystal stretching, splitting, and retracting.

Under the electron beam irradiation, AgCl immersed in water is known to decompose into Ag and  $\text{HCl}$ .<sup>[4–6,9]</sup> However, in our experiments, a Ag oxidation process must be accompanied by the  $\text{Ag}^+$  reduction since no obvious Ag plating was observed. It is well established that radiolysis of water under the electron beam generates hydrated electrons, protons, and oxidative hydrogen peroxides, which could induce redox reactions of AgCl:



The reverse reaction of Ag oxidation into AgCl consumes the  $\text{H}^+$  near the nanocrystals. Given the fact that the produced  $\text{H}^+$  diffuses much faster than  $\text{Cl}^-$  in the forward reaction, a  $\text{Cl}^-$  rich inside/ $\text{H}^+$  rich outside ionic gradient is formed. A dynamic equilibrium preventing the AgCl nanocrystals from decomposition into Ag metals can be established. The estimated ion distribution around the AgCl nanocrystal under the dynamic equilibrium is illustrated in Figure 5a. The surface of AgCl nanocrystals is known to be easily adsorbed with  $\text{Cl}^-$  due to strong  $\text{Ag}^+ \text{--} \text{Cl}^-$  affinity on the first Helmholtz layer, and be further screened by outer layer ions (e.g.,  $\text{H}^+$ ).<sup>[19–21]</sup>

The reshaping and splitting dynamics of AgCl nanocrystals fits well with Rayleigh's instability theory on Coulomb fission. Coulomb fission was first reported on electrified droplets,<sup>[22–25]</sup> which become unstable with a critical charge  $Q_c$  (known as Rayleigh limit) when the repulsive Coulomb force is equal to the cohesive surface tension. Recent high-speed optical microscopy studies have revealed the detailed Coulomb fission dynamics of a liquid droplet.<sup>[26–28]</sup> Coulomb fission has also been applied to a variety of charged solids, spanning from femtometer structures

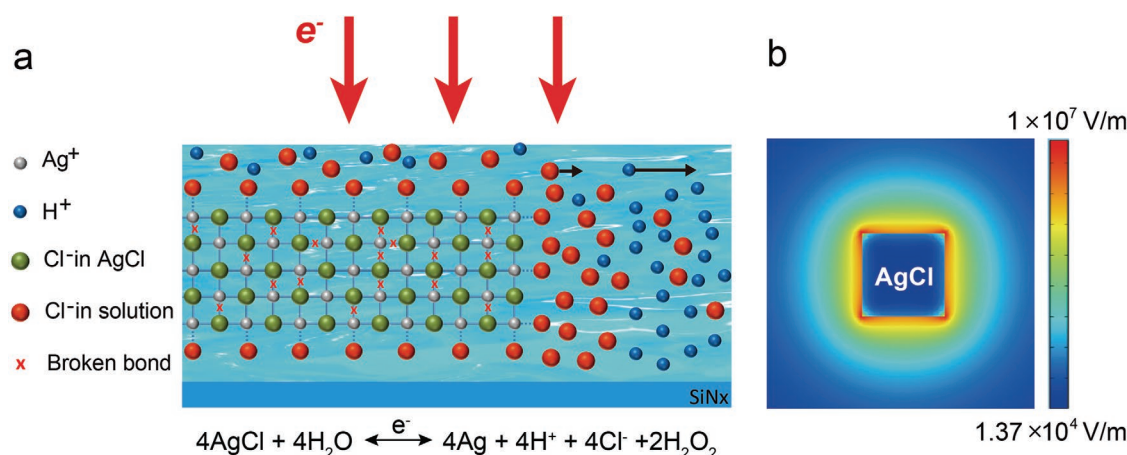


**Figure 5.** Mechanisms of Coulomb fission of AgCl nanoparticles in an aqueous solution under electron beam illumination. a) Schematic of AgCl redox reaction in KCl solution under an electron beam. The reaction equation combines the AgCl decomposition due to the electron beam illumination and recovery due to oxidants ( $\text{H}_2\text{O}_2$ ) generated by the interaction of electron beam with water. The arrows on  $\text{Cl}^-$  and  $\text{H}^+$  show the difference in diffusion speed resulting in an electrolyte gradient. b) Finite element method (FEM) simulation of electric field distribution assuming an evenly distributed surface charge with a charge density of  $0.327 \text{ e nm}^{-2}$ .

of nuclei (e.g., radium-228)<sup>[29,30]</sup> to nanometer structures of large molecules (e.g., proteins),<sup>[31,32]</sup> metal clusters (e.g., gold or sodium clusters),<sup>[33–35]</sup> and carbon-based materials (e.g., fullerene or nanotubes).<sup>[36–38]</sup> A similar Coulomb fission model can be applied to the observed electron beam induced splitting of AgCl nanocrystals. When the adsorbed charges reach the Rayleigh limit, explosive Coulomb fission results in drastic ejection of the charges and splitting of the nanocrystal into smaller pieces. After splitting, charges on the original nanocrystal are distributed on the smaller pieces. Thus, the overall electrostatic energy decreases due to the charge redistribution, whereas the surface energy increases due to increased surface area. Surface tension dominates the smaller pieces and it retracts the irregular shaped particles into nanocuboids. The larger nanocrystals exhibiting the mild splitting events, such as the cases in Figure 1d, may be induced by non-uniform surface charges and/or surface tension and defects inside the nanocrystal may have played a role.

In order to quantify the scale of electrostatic repulsion, we use the finite element method (FEM) to simulate the electric field distribution of a AgCl nanocrystal in KCl solution. We assume an evenly distributed surface charge density allowing the average electrostatic force equals the surface tension. Our simulation shows that the edges and corners of the nanocrystal experience the maximum electric field (Figure 5b). This explains why stretching originates from the corners of a nanocrystal. When the repulsive force is larger than the surface tension, the AgCl nanocrystal becomes unstable and the spontaneous reshaping and stretching of AgCl nanocrystals can be achieved.

We further analyze the morphological transition of AgCl from a round nanoparticle into a more faceted nanocuboid from the viewpoint of Gibbs free energy (such as the case in Figure 3a). The Gibbs free energy change of the system  $\Delta G$  can be expressed by:

$$\Delta G = \Delta E_C + \Delta E_\sigma + \Delta E_V = \Delta Q^2 / 2C_s + \sigma \Delta A + \Delta E_V \quad (2)$$

where,  $E_C$  is the Coulomb energy,  $E_\sigma$  is the interfacial free energy,  $E_V$  is the bulk free energy of the AgCl crystal,  $Q$  is the charge amount on a nanocrystal,  $\sigma$  is the surface tension.  $C_s$  and  $R_s$  are the capacitance and equivalent radius of the ball-like AgCl nanocrystals (see Section S1, Supporting Information). During splitting,  $\Delta E_C$  is negative and  $\Delta E_\sigma$  is positive.  $\Delta E_V$  is positive because any reshaping in solid materials should overcome an energy barrier. But due to the electron beam induced radiolysis, the AgCl NCs exhibit liquid-like behaviors where the strong ionic bonds are already massively broken. Here, we approximate the critical charge by assuming  $\Delta E_V$  is zero. For example, for a nanocrystal with radius of 50 nm, the minimum charge is 10980e, which equals to a charge density of 0.31 e nm<sup>-2</sup>. Whereas the critical charge for a nanocrystal with radius of 25 nm is 3882e, which equals to a charge density of 0.44 e nm<sup>-2</sup>. The smaller nanocrystals require a higher charge density to reshape and split.

## 5. Conclusion

In summary, we have observed spontaneous reshaping and splitting of single crystalline AgCl nanocrystals using liquid

cell TEM. The results show that AgCl nanocrystals maintain the single crystal lattice during the splitting event. The reshaping and splitting of AgCl arise from the interplay between the repulsive electrostatic force and the cohesive surface tension. The directional splitting of AgCl nanocrystals initiated at the corners is distinctly different from the splitting of electrified droplets or other reported Coulomb fission, while high flexibility of the AgCl nanocrystal is observed. This work opens the opportunity to further study Coulomb fission of solids and explore potential applications as actuators in nanodevices.

## 6. Experimental Section

**Liquid Cells and Instruments:** An in situ fluid stage (Hummingbird Scientific, USA) was used in this experiment. No spacer is applied on the SiN<sub>x</sub> windows, but due to the surface is not perfectly clean, a liquid layer of 100–200 nm was usually obtained. All the in situ experiments were carried out using a JEOL 2010F microscope operating at 200 keV. A bubble in the middle of the SiN<sub>x</sub> window was formed to introduce a thin liquid region.

**Preparation of AgCl Nanocrystals:** The AgCl was formed by immersing silver nanocrystals in potassium chloride (KCl) solution. The silver nanocrystals were formed by depositing 1 nm silver onto the SiN<sub>x</sub> membrane of SiN<sub>x</sub> chip using thermal evaporator.<sup>[39]</sup> Then KCl solution was loaded into the liquid cell. Under electron irradiation, chloride ions facilitate the oxidative dissolution of silver and AgCl precipitates near the SiN<sub>x</sub> membrane.<sup>[40]</sup> The concentration of the KCl solution we used was 10 × 10<sup>-3</sup>, 25 × 10<sup>-3</sup>, 40 × 10<sup>-3</sup>, and 100 × 10<sup>-3</sup> M. All four concentrations ensure a chloride-excess environment. No obvious difference was observed.

**Electric Field Simulation:** Poisson equation was applied based on the simulation software COMSOL to simulate the electric field distribution. The surface charge density was set to be Rayleigh limit, which is 0.052 C m<sup>-2</sup>, or 0.327 e nm<sup>-2</sup>. The static dielectric constant of AgCl at room temperature is 11.14. The static dielectric constant of 10 × 10<sup>-3</sup> M KCl at room temperature is 78. More details are in Section S4 (Supporting Information).

## Supporting Information

Supporting Information is available from the Wiley Online Library or from the author.

## Acknowledgements

This work was funded by U.S. Department of Energy, Office of Science, Office of Basic Energy Sciences, Materials Sciences and Engineering Division under Contract No. DE-AC02-05-CH11231 within the in situ TEM program (KC22ZH). X.Z. acknowledges the support of SinBeRise program of Berkeley Education Alliance for Research in Singapore (BEARS). U.M. acknowledges the supports from the Singapore Ministry of Education under Academic Research Fund Tier 2 (MOE2016-T2-2-009). X.T. thanks Jingyu Lu, Zainul Aabdin and Qi Liu for their help with the guidance on experimental set up.

## Conflict of Interest

The authors declare no conflict of interest.



## Keywords

AgCl nanomotors, charged nanocrystals, in situ transmission electron microscope, liquid cell, shape instability

Received: August 10, 2018

Revised: September 9, 2018

Published online: October 7, 2018

- [1] P. Illien, R. Golestanian, A. Sen, *Chem. Soc. Rev.* **2017**, 46, 5508.
- [2] M. Safdar, J. Simmchen, J. Janis, *Environ. Sci.: Nano* **2017**, 4, 1602.
- [3] L. Xu, F. Mou, H. Gong, M. Luo, J. Guan, *Chem. Soc. Rev.* **2017**, 46, 6905.
- [4] A. Sen, M. Ibele, Y. Hong, D. Velegol, *Faraday Discuss.* **2009**, 143, 15.
- [5] I. Michael, M. T. E. , S. Ayusman, *Angew. Chem., Int. Ed.* **2009**, 48, 3308.
- [6] W. Duan, M. Ibele, R. Liu, A. Sen, *Eur. Phys. J. E* **2012**, 35, 77.
- [7] J. L. Anderson, *Annu. Rev. Fluid Mech.* **1989**, 21, 61.
- [8] C. Zhou, H. P. Zhang, J. Tang, W. Wang, *Langmuir* **2018**, 34, 3289.
- [9] M. E. Ibele, P. E. Lammert, V. H. Crespi, A. Sen, *ACS Nano* **2010**, 4, 4845.
- [10] H. Zheng, R. K. Smith, Y.-w. Jun, C. Kisielowski, U. Dahmen, A. P. Alivisatos, *Science* **2009**, 324, 1309.
- [11] U. M. Mirsaidov, H. Zheng, D. Bhattacharya, Y. Casana, P. Matsudaira, *Proc. Natl. Acad. Sci. USA* **2012**, 109, 7187.
- [12] H.-G. Liao, D. Zherebetsky, H. Xin, C. Czarnik, P. Ercius, H. Elmlund, M. Pan, L.-W. Wang, H. Zheng, *Science* **2014**, 345, 916.
- [13] Z. Zeng, W.-I. Liang, H.-G. Liao, H. L. Xin, Y.-H. Chu, H. Zheng, *Nano Lett.* **2014**, 14, 1745.
- [14] Z. Lou, B. Huang, X. Ma, X. Zhang, X. Qin, Z. Wang, Y. Dai, Y. Liu, *Chem. - Eur. J.* **2012**, 18, 16090.
- [15] H. R. Lillie, *J. Rheol.* **1932**, 3, 121.
- [16] T. Tani, *Photographic Science: Advances in Nanoparticles, J-Aggregates, Dye Sensitization, and Organic Devices*, Oxford University Press, Oxford **2011**.
- [17] D. B. Williams, C. B. Carter, *Transmission Electron Microscopy: A Text-book for Materials Science*, Springer, New York **2009**.
- [18] L. Reimer, H. Kohl, *Transmission Electron Microscopy: Physics of Image Formation*, Springer, New York **2008**.
- [19] K. R. Tersamany, K. Lu Cheng, *Sens. Actuators, B* **2001**, 76, 551.
- [20] K. L. Cheng, *Microchem. J.* **2002**, 72, 269.
- [21] H. Tamagawa, S. Morita, *Membranes* **2014**, 4, 257.
- [22] L. Rayleigh, *London Edinburgh Dublin Philos. Mag. J. Sci.* **1882**, 14, 184.
- [23] C. D. Hendricks, *J. Colloid Sci.* **1962**, 17, 249.
- [24] A. Doyle, D. R. Moffett, B. Vonnegut, *J. Colloid Sci.* **1964**, 19, 136.
- [25] D. C. Taffin, T. L. Ward, E. J. Davis, *Langmuir* **1989**, 5, 376.
- [26] K. Tang, A. Gomez, *Phys. Fluids* **1994**, 6, 2317.
- [27] T. Achtzehn, R. Müller, D. Duft, T. Leisner, *Eur. Phys. J. D* **2005**, 34, 311.
- [28] D. Duft, T. Achtzehn, R. Muller, B. A. Huber, T. Leisner, *Nature* **2003**, 421, 128.
- [29] S. Frankel, N. Metropolis, *Phys. Rev.* **1947**, 72, 914.
- [30] P. Moller, D. G. Madland, A. J. Sierk, A. Iwamoto, *Nature* **2001**, 409, 785.
- [31] J. Jortner, I. Last, Y. Levy, *Int. J. Mass Spectrom.* **2006**, 249-250, 184.
- [32] M. Vonderach, O. T. Ehrler, K. Matheis, T. Karpuschkin, E. Papalazarou, C. Brunet, R. Antoine, P. Weis, O. Hampe, M. M. Kappes, P. Dugourd, *Phys. Chem. Chem. Phys.* **2011**, 13, 15554.
- [33] F. Chandezon, S. Tomita, D. Cormier, P. Grubling, C. Guet, H. Lebius, A. Pesnelle, B. A. Huber, *Phys. Rev. Lett.* **2001**, 87, 153402.
- [34] F. Calvo, *Phys. Rev. A* **2006**, 74, 043202.
- [35] M. Bär, B. Faber, P. G. Reinhard, P. M. Dinh, E. Suraud, P. Wopperer, *J. Phys.: Conf. Ser.* **2010**, 248, 012023.
- [36] G. Liu, Y. Zhao, K. Zheng, Z. Liu, W. Ma, Y. Ren, S. Xie, L. Sun, *Nano Lett.* **2009**, 9, 239.
- [37] A. J. Stace, E. Bichoutskaia, *Phys. Chem. Chem. Phys.* **2011**, 13, 18339.
- [38] X. Wei, D.-M. Tang, Q. Chen, Y. Bando, D. Golberg, *ACS Nano* **2013**, 7, 3491.
- [39] C. Binns, *Surf. Sci. Rep.* **2001**, 44, 1.
- [40] K. Loza, J. Diendorf, C. Sengstock, L. Ruiz-Gonzalez, J. M. Gonzalez-Calbet, M. Vallet-Regi, M. Koller, M. Eppe, *J. Mater. Chem. B* **2014**, 2, 1634.